HHS Public Access

Author manuscript

Neurobiol Dis. Author manuscript; available in PMC 2022 June 15.

Published in final edited form as:

Neurobiol Dis. 2022 June 15; 168: 105701. doi:10.1016/j.nbd.2022.105701.

Differences in hippocampal plasticity and memory outcomes in anterior versus posterior cerebellar stroke

Myriam Moreno[1], **Crystal Minjarez**[1], **Jose Vigil**[1], **James E Orfila**[1], **Roxanna Schmidt**[2], **Amelia Burch**[1], **Danelle J Carter**[1], **Molly Kubesh**[1], **Joan Yonchek**[3], **Robert M Dietz**[4], **Nidia Quillinan**[5]

[1]Department of Anesthesiology, 12801 E. 17th Ave. MS8130, Research 1 South, Aurora, CO 80045, USA; Neuronal Injury and Plasticity Program, 12801 E. 17th Ave. MS8130, Research 1 South, Aurora, CO 80045, USA.

[2]Neuronal Injury and Plasticity Program, 12801 E. 17th Ave. MS8130, Research 1 South, Aurora, CO 80045, USA.

[3]Department of Anesthesiology, 12801 E. 17th Ave. MS8130, Research 1 South, Aurora, CO 80045, USA.

[4]Neuronal Injury and Plasticity Program, 12801 E. 17th Ave. MS8130, Research 1 South, Aurora, CO 80045, USA; Department of Pediatrics, University of Colorado Anschutz Medical Campus, Aurora, CO, USA.

[5]Department of Anesthesiology, 12801 E. 17th Ave. MS8130, Research 1 South, Aurora, CO 80045, USA; Neuronal Injury and Plasticity Program, 12801 E. 17th Ave. MS8130, Research 1 South, Aurora, CO 80045, USA.

Abstract

Neurological symptoms following cerebellar stroke can range from motor to cognitive-affective impairments. Topographic imaging studies from patients with lesions confined to the cerebellum have shown evidence linking anterior cerebellar lobules with motor function and posterior lobules with cognitive function. Damage to the cerebellum can disrupt functional connectivity in cerebellar stroke patients, as it is highly interconnected with forebrain motor and cognitive areas. The hippocampus plays a key role in memory acquisition, a cognitive domain that is negatively impacted by posterior cerebellar stroke, and there is increasing evidence that the

*Corresponding author at: Department of Anesthesiology, University of Colorado, Anschutz Medical Campus, 12801 East 17th Avenue, Rm 4105, Aurora, CO 80045, USA. nidia.quillinan@cuanschutz.edu (N. Quillinan).

Disclosures

None.

CRediT authorship contribution statement

Myriam Moreno: Methodology, Investigation, Formal analysis, Visualization, Writing – original draft. **Crystal Minjarez:** Investigation. **Jose Vigil:** Investigation, Validation, Writing – review & editing. **James E. Orfila:** Investigation. **Roxanna Schmidt:** Methodology, Investigation. **Amelia Burch:** Investigation. **Danelle J. Carter:** Validation. **Molly Kubesh:** Methodology, Investigation. **Joan Yonchek:** Methodology. **Robert M. Dietz:** Investigation, Writing – review & editing. **Nidia Quillinan:** Conceptualization, Supervision, Funding acquisition.

Appendix A. Supplementary data

Supplementary data to this article can be found online at https://doi.org/10.1016/j.nbd.2022.105701.

cerebellum can affect hippocampal function in health and disease. To study these topographical dissociations, we developed a mouse photo-thrombosis model to produce unilateral strokes in anterior (lobules III-V) or posterior (lobules VI-VIII) cerebellar cortex to examine hippocampal plasticity and behavior. Histological and MRI data demonstrate reproducible injury that is confined to the targeted lobules. We then measured hippocampal long-term potentiation (LTP) ex-vivo with extracellular field recording experiments in acute brain slices obtained from mice 7 days post-cerebellar stroke. Interestingly, we found that a unilateral posterior stroke resulted in a contralateral hippocampal impairment, matching the cerebellothalamic pathway trajectory, while LTP was intact in both hippocampi of mice with anterior strokes. We also assessed motor coordination and memory function at 7 days post-stroke using a balance beam, contextual and delay fear conditioning (CFC and DFC), and novel object recognition (NOR) tasks. Mice with anterior strokes showed lack of coordination evaluated as an increased number of missteps, while mice with posterior strokes did not. Mice with anterior or posterior cerebellar strokes demonstrated similar freezing behavior to shams in CFC and DFC, while only posterior stroke mice displayed a reduced discrimination index in the NOR task. These data suggest that a unilateral LTP impairment observed in mice with posterior strokes produces a mild memory impairment. Our results demonstrate that our model recapitulates aspects of clinical lesion-symptom mapping, with anterior cerebellar strokes producing impaired motor coordination and posterior cerebellar strokes producing an object-recognition memory impairment. Further studies are warranted to interrogate other motor and cognitive-affective behaviors and brain region specific alterations following focal cerebellar stroke. The novel model presented herein will allow for future preclinical translational studies to improve neurological deficits after cerebellar stroke.

Keywords

Cerebellar stroke; Long-term potentiation; Electrophysiology; Motor impairment; Cerebellar cognitive-affective syndrome

1. Introduction

Stroke is a leading cause of death and disability worldwide. In the United States over 795,000 cases are reported annually and approximately 85% of these cases are the result of vessel occlusion (Guzik and Bushnell, 2017). The risk factors include advanced age, diabetes mellitus, hypertension, coronary artery disease, elevated lipids and smoking (Hankey, 2017). Although occlusion of forebrain arteries is most common, cerebellar strokes account for nearly 25,000 strokes every year and have a disproportionally high mortality rate when compared to other strokes (Macdonell et al., 1987). The cerebellum receives an arterial blood supply from the superior, posterior-inferior and anterior-inferior cerebellar arteries. Occlusion of any of these arteries due to ischemia, particularly of the superior cerebellar arteries (SCA), can have an impact on motor and cognitive function (Kim et al., 2016). Acute clinical symptomatology can be non-specific and resemble many other disorders (Edlow et al., 2008) making cerebellar stroke difficult to diagnose within the therapeutic window for anti-thrombolytics and endovascular therapy. If cerebellar stroke therapies are to be developed, an understanding of long-term mechanisms of motor and

cognitive impairments is needed. Currently, there are no studies that have investigated the behavioral and network alterations that occur after cerebellar stroke.

Motor and vestibular symptoms after cerebellar stroke have been long recognized in clinical cases, but it is only within the last two decades that cognitive deficits associated with cerebellar stroke have become appreciated (Schmahmann, 1996; Schmahmann et al., 2009; Stoodley et al., 2012; Koziol et al., 2014; Bodranghien et al., 2016; Stoodley et al., 2016; Stoodley and Schmahmann, 2018). Clinical research (symptomatology and fMRI lesion-mapping) performed on patients with either stroke or tumorigenic lesions confined to the cerebellum, have revealed a difference between processes regulated by anterior and posterior lobules of the cerebellum. These studies show that patients with an injury to anterior lobules of the cerebellum display ataxia, dysmetria, vertigo, and other motor coordination and motor learning impairments, while patients with lesions to posterior lobules display memory, language, visual-spatial, emotional and executive dysfunctions (Schmahmann, 1996; Stoodley and Schmahmann, 2018). Despite well-documented data of the cerebellar involvement in cognitive-affective processes (Schmahmann, 1996; Desmond and Fiez, 1998; Strick et al., 2009; Stoodley et al., 2012; Buckner, 2013; Rochefort et al., 2013; Koziol et al., 2014; Kim et al., 2016; Stoodley and Schmahmann, 2018), the precise functional networks and anatomical pathways the cerebellum uses to modulate cognition are far less understood.

The hippocampus plays a key role in memory formation and synaptic plasticity in the hippocampus is a cellular mechanism that underlies this function. Damage to the posterior region of the cerebellum can impair memory function (Stoodley et al., 2016), but it is still not well understood how disruptions in the hippocampal network contribute to cognitive dysfunction. Functional topography studies in the human cerebellum have established reciprocal connectivity of the cerebellum with sensory-motor and associative cortices (Strick et al., 2009; Stoodley et al., 2012). Optogenetic fMRI, electrophysiological identification and multiple tracing studies in animal models have shown indirect connectivity and anatomical correlates of cerebellar-hippocampal connectivity (Krook-Magnuson et al., 2014; Igloi et al., 2015; Choe et al., 2018; McAfee et al., 2019; Zeidler et al., 2020). Therefore, we hypothesize that cerebellar-induced changes in hippocampal function may contribute to memory deficits observed in cerebellar stroke patients with posterior localized cerebellar strokes. To test this hypothesis, we performed photo-thrombosis to induce focal cerebellar strokes in anterior or posterior lobules of the mouse cerebellar cortex and evaluated hippocampal plasticity, memory and motor coordination.

2. Materials and methods

2.1. Animals

All experimental protocols were approved by the Institutional Animal Care and Use Committee (IACUC) at the University of Colorado and adhered to the National Institute of Health guidelines for the care and use of animals in research. Male and female, 8–12 weeks-old, C57BL/6 mice were purchased from Charles River Laboratories (CRL). All mice were permitted access to water and standard lab chow ad libitum with a 14/10-h light/dark cycles.

2.2. Photo-thrombotic surgery

Animals were anesthetized and kept at 2% isoflurane (20% oxygen/80% room air) and placed on a stereotaxic frame with a rectal temperature controller (36.5° ± 0.3 °C) and eye lubrication. The scalp was properly disinfected and treated with bupivacaine at 10 mg/mL prior to incision. A scalp incision was performed at the level of lambda and trapezius muscle was gently detached from the interparietal bone and lowered to visualize the left superior cerebellar artery (SCA). The bone overlying the SCA was thinned out with micromotor drill (Foredom) with a 2-mm rounded-head drill bit. Different lobules were targeted by changing the angle and position of the fiberoptic cold LED white source (diameter: 1.5 mm, Thorlabs) (Fig. 1c and Supplementary Fig. IIa). To generate a posterior cerebellar stroke the light was positioned above the SCA covering portions of lobules VI-VIII. For anterior cerebellar strokes the light was positioned at lobules IV-V (See Supplementary Figure Ia). Rose Bengal (RB) (Sigma-Aldrich) was administered intraperitoneally (150 μg/g) prior to illumination. Illumination was localized at the bone thinning location (touching the skull) and turned on 5 min post-RB injection and was maintained for 15 min. The scalp was glued closed and treated with a topical triple antibiotic ointment and lidocaine, followed by a subcutaneous injection of 500 μL of 0.9% saline after the surgery was completed. Mice were housed individually over a heating pad at 35 °C overnight and allowed to recover for 1 or 7 days. Sham animals underwent the same procedure as our stroke animals except for administration of RB, ruling out any possible damage due to light exposure alone. Mice with anterior and posterior strokes had similar mortality rates, 14 out of 126 (11.11%) animals with posterior strokes and 5 out of 51 (9.8%) animals with anterior strokes died within 1–3 days after surgery.

2.3. Vasculature visualization

For vasculature visualization, naïve animals were perfused with black India ink (Pelikan Black Fountain Ink) diluted at a 1:1 ratio with 1× phosphate buffered saline (PBS) at a rate of 5 mL/s for 2mins (Supplementary Fig. Ia). The brain was collected and imaged with a light microscope to allow for visualization of the SCA.

2.4. Histology

Mice were transcardially perfused at 1- or 7-days post-surgery with 1× PBS followed by 4% paraformaldehyde (PFA) for tissue fixation, sectioning and staining. Cerebellums were paraffin embedded and 6 μm sections were prepared. A total of approximately 240 slides were obtained and 4 slide sets were generated, each set with 24 sections at 30 um intervals mounted onto 4 slides. One slide set (4 slides total) was stained with hematoxylin and eosin (H&E), while the other 3 slides of the set (12 slides total) were used for immunohistochemistry (IHC).

2.5. Stereology

For quantification of infarct volume, one set of H&E stained 6-μm paraffin sections was used for stereological analysis. A Leica photomicroscope (Leica Microsystems) and *StereoInvestigator* program (Stereologer 2000, SRC) were used for this analysis. A total of

12 standardized sections were analyzed per animal. Infarcted tissue was traced onto a point grid at 1.25× magnification, and tissue depth was calculated at 40× magnification.

Stereologer software calculated global infarct volume in cubic micrometers according to the Cavalieri principle and volumes were converted into cubic microns.

2.6. Blood-brain barrier permeability

Evans blue was used at a concentration of 2% in 0.9% saline solution and injected intraperitoneally 4 h before perfusion of sham and stroke animals. Mice were perfused with 1 × PBS and cerebellums were collected for qualitative analysis and visualization of the cerebellar cortex. For quantitative analysis of BBB disruption, ovalbumin conjugated to Alexa Fluor-647 (Molecular Probes by Life Technologies) was retro-orbitally injected into sham and cerebellar stroke animals at a concentration of 1% in 0.9% saline 4 h before perfusion with 1× PBS/4% PFA. Cerebellums were then collected and post-fixed in 4% PFA for 1 day and then transferred to a cryo-protection solution containing 30% sucrose. Cerebellums were cryo-sectioned at a 30-μm thickness and prepared for a free-floating section IHC protocol. To visualize ovalbumin extravasation, sections were co-stained with a rabbit anti-Glut1 antibody (ThermoScientific RB-9052-P) at a concentration of 1:500 to label endothelial cells followed by an anti-rabbit secondary antibody conjugated with Alexa Fluor-488. Sections were then mounted and imaged at 647 nm (ovalbumin) and 488 nm (Glut-1) wavelengths with a 40× objective using epifluorescent microscope with Qcapture Pro software. Percent area of positive pixels was averaged from 4 images per side per animal for shams and from 5 images per side (ipsilateral and contralateral) per stroke animals. Images with merged channels were used for representative ovalbumin visualization while only 647 channel images were processed for ovalbumin quantification. The ovalbumin signal was quantified based on area percentage of ROI (entire image) after applying a standard intensity threshold filter (triangle white) across images with a Fiji macro.

2.7. Immunohistochemistry

An immunohistochemistry (IHC) protocol was performed as previously described by (Dingman et al., 2019; Orfila et al., 2019) to evaluate the cerebellum and hippocampus. Neuronal nuclei and reactive microglia and astrocytes were evaluated with NeuN (Millipore, MAB377, 1:500), glial fibrillary acidic protein (GFAP, Santa Cruz SC33673, 1:500) and Iba-1 (Wako, 019–19,741, 1:500), respectively. Secondary antibodies raised in donkey and conjugated to Alexa Fluor-488, 594 or 647 (Jackson Immunoresearch) were used at a dilution of 1:600. For cerebellum, 6 sections per animal were stained. Images were acquired from the peri-infarct area (molecular layer), 3 images at 40× were obtained per side for each cerebellar slice for a total of 12 images per animal. For hippocampus, images were acquired in the CA1 region from 3 sections per animal. Percentage of positive pixels was analyzed based on area percentage of ROI (entire image) after applying a standard intensity threshold filter (triangle white) across images with a Fiji macro.

2.8. Laser speckle imaging

Images of SCA blood flow were acquired in a small subset of posterior and anterior cerebellar strokes using a laser speckle imager (RWD Life Sciences). Animals underwent

standard photothrombotic procedure. The skull was moistened with saline to facilitate imaging and the laser speckle camera was positioned approximately 6 in. above the skull. Static images were acquired immediately before and 5 min after photoillumination of the targeted portions of the SCA.

2.9. Behavioral testing

Testing was performed 7 days after sham or stroke surgery. Mice were transported in their home cages to a behavioral suite and allowed to habituate for 30 min prior to testing. Motor coordination was tested with a balance beam and memory with a contextual fear and delay fear conditioning (CFC/DFC) assay and novel object recognition (NOR). Open field, balance beam and CFC were performed in the same cohorts while separate cohorts were used for DFC and NOR tasks.

Motor testing (balance beam).—A tapered, elevated balance beam (165 cm) was used to assess motor coordination. The beam is tapered in width from 1.2 cm at the start point to 0.5 cm at the stop point with a ledge running the length of either side of the beam that is 2 cm below the level of the beam and 1.5 cm wide (Carter et al., 2001). A dark goal box (10.5 × 10.5 × 10.5 cm) positioned at one end of the beam. Mice were trained to cross the balance beam without turning around or pausing to explore (5–10 trials). Once trained, 3 sessions were recorded and videos were analyzed for number of missteps or slips onto the ledge (Schaar et al., 2010).

CFC.—Memory performance was evaluated by using a CFC assay. Mice are placed in a silent behavioral room for habituation for 30 min in their own home cage prior to the testing. Mice were then taken out of their home cage into an empty bucket for 2 mins and then placed into a chamber with a metal-based platform for another 2 mins for habituation and development of associative memory. A 1 mA current was then delivered through the metal-based platform for 1 s. The current produces a mild electric shock to their paws, perceived as an aversive stimulus. Mice were then re-introduced to the same context (environment) 24 h later. Freezing behavior was evaluated over the first 5 min by observing mouse behavior every 10 s and scored as freezing or not freezing. Freezing behavior is a sign of intact memory association between environmental cues and an aversive stimulus experienced the day before. CFC was performed prior to balance beam motor testing.

DFC.—A fear conditioning apparatus was used consisting of a sound attenuating chamber (24”L × 14”W × 14”H), which contained a grid-shock floor (Coulbourn Instruments, P/N H10–11 M-TC) onto which a Plexiglas cube (6 × 6 × 6) was placed to contain the mice during the experiments (Context A). The shock floor was connected to an animal shocker that was automatically triggered by an Arduino control board. The conditioned stimulus (CS) was a 15 s tone (60 dB) delivered by a piezo buzzer (McMaster-Carr) that co-terminated with foot-shock (0.5 mA, 1 s) (unconditioned stimulus – US). For all procedures carried out in Context A, the apparatus was cleaned with a 70% isopropanol solution before and after each animal, and each animal was transported to the conditioning room in their home-cage. Context B consisted of a white bucket (7″ diameter, 7″ tall) loosely covered by a clear Plexiglas sheet and placed into the sound attenuating chamber. A small vial

containing vanilla extract was placed in the corner of the sound attenuating chamber and the apparatus was cleaned with a 70% ethanol solution before and after each animal. For all procedures carried out in Context B, the animals were individually transported to the conditioning room in small, empty, white square containers. Any-maze software (Stoelting) was used to record and assess freezing behavior during every stage of the procedure. On the first day of the procedure, animals were habituated to the conditioning room while in their home cage for one hour. Animals were also habituated to Context A for 5-min without presentation of the CS or the US. 24-h later, animals were re-exposed to Context A to obtain a 2-min baseline before CS/US pairing. After the baseline period, three CS/US pairings were delivered with 1-min separating each pairing. After the last CS/US pairing, mice were allowed to remain in the chamber for 1 min and 45 s before being returned to their home cage. The next day, animals were returned to context A for 2-min without presentation of CS or US to assess contextual fear. The following day, animals were transported to the conditioning room in novel containers and exposed to the novel context B for 2-min. After this baseline period, the CS was delivered to assess cued fear. Mice were allowed to remain in context B for an additional 1.5 min after CS presentation before being returned to their home cage.

NOR.—NOR was performed in a 3-chamber apparatus (24.75”W × 16.75″ L × 8.75”H; each chamber was 7″ in length) with open doorways between chambers. Mice were habituated to the room for 1 h. Mice were then placed into the center chamber of the apparatus with identical objects placed in the outer chambers and allowed to explore the box and objects for 10 min. Mice were returned to their home cage for 30 min before undergoing a second trial. The second trial consisted of placing an object from trial one on one end of the three-chamber box, and a new object on the opposite end. Mice explored these objects and environment for another 10 min before being returned to their home cage. Data was recorded and analyzed in Any-Maze and time spent exploring each box is converted into a discrimination index for: (Novel object - Familiar Object) / (Novel object + Familiar Object). Data are reported as the difference in discrimination index between trial 1 and trial 2.

2.10. In vivo MRI

All non-invasive MRI protocols were developed at the Colorado Animal Imaging Shared Resource (AISR) on an ultra-high field Bruker 9.4 Tesla BioSpec MR scanner (Bruker Medical) equipped with a mouse head-array RF cryo-coil. Briefly, the mouse was anesthetized with 2% isoflurane and placed on a temperature-controlled animal bed. Non-gadolinium multi-sequential MRI protocol was applied to acquire (i) high-resolution T2-weighted turboRARE (***R****apid* ***A****cquisition with* ***R****elaxation* ***E****nhancement*, 52 μm in-plane resolution); and (ii) axial fast spin echo DWI (***D****iffusion* ***W****eighted* ***I****maging*) with six b-values for tumor cellularity and edema. All MRI acquisitions and image analysis were performed using Bruker ParaVision 360NEO software. For volumetric assessments, free-hand drawn regions of interests (ROIs) were placed over the injury or edema region on each sagittal slice. The total injury or edema volume was reported in mm^3 as the sum of all ROIs from individual slices multiplied by a slice thickness (0.7 mm, no slice gap). Oval or circular

ROI were used for DWI analysis and calculations of the apparent diffusion coefficients (ADCs) in the injured regions.

2.11. Hippocampal electrophysiology

Acute hippocampal slice preparation.—Hippocampal slices were prepared at 7 days after recovery from cerebellar stroke or sham surgeries. Mice were anesthetized with 3% isoflurane in an O_2-enriched chamber. Mice were transcardially perfused with ice-cold (2–5 °C) oxygenated (95% O2/5% CO_2) artificial cerebral spinal fluid (aCSF) for 2 min prior to decapitation. The brains were then extracted and sectioned in aCSF. The composition of aCSF was the following (in mmol/L): 126 NaCl, 2.5 KCl, 25 $NaHCO_3$, 1.3 NaH_2PO_4, 2.5 $CaCl_2$, 1.2 $MgCl_2$, and 12 glucose. Horizontal hippocampal slices (300 μm thick) were cut with a Vibratome VT1200S (Leica) and transferred to a holding chamber containing room temperature aCSF for at least 1 h before recording (Dietz et al., 2018).

Extracellular field potential recordings.—Synaptically evoked field potentials were recorded from hippocampal CA1 slices that were placed on a temperature controlled (31 ± 0.5 °C) interface chamber perfused with aCSF at a rate of 1.5 mL/min. Field excitatory post-synaptic potentials (fEPSP) were produced by stimulating the Schaffer collaterals (CA3 axons) and recording in the stratum radiatum of the CA1 region. Analog fEPSPs were amplified (1000×) and filtered through a preamplifier (Model LP511 AC, Grass Instruments) at 1.0 kHz, digitized at 10 kHz and stored on a computer for later off-line analysis (Clampfit 10.4, Axon Instruments). The derivative (dV/dT) of the fEPSP rise slope was measured. The fEPSPs were adjusted to 50% of the maximum slope and test pulses were evoked every 20 s. Paired pulse responses were recorded using a 50-ms interpulse interval (20 Hz) and expressed as a ratio of the slopes of the second pulse over the first pulse. A 20-min stable baseline was established before delivering a theta burst stimulation (TBS) train of four pulses delivered at 100 Hz in 30-ms bursts repeated 10 times with 200-ms interburst intervals. Following TBS, the fEPSP was recorded for 60 min. The averaged 10-min slope from 50 to 60 min after TBS was divided by the average of the 10-min baseline (set to 100%) prior to TBS to determine the amount of potentiation. For time course graphs, normalized fEPSP slope values were averaged and plotted as the percent change from baseline.

2.12. Rigor and statistics

Experiments were performed in accordance to the ARRIVE 2.0 guidelines (Kilkenny et al., 2010; Percie du Sert et al., 2020). All animals were given a blinded code before behavior or electrophysiology was performed. Animals were excluded from behavioral or electrophysiological analysis if there was no detectable infarct on histological assessment or if baseline freezing of greater than 20%, indicative of increased generalized fear, was observed on day 1 of CFC task. All graphs and statistics were generated on Graphpad Prism 9. Normality criteria was determined per group and data set using the Shapiro-Wilks' test. Two group comparisons were performed using unpaired student *t*-test or the Mann-Whitney, 2 T method. Data consisting of three or more groups were evaluated by a one-way or two-way ANOVA (parametric) or the Kruskal-Wallis test (non-parametric). Multiple comparisons correction test was run for applicable data sets, indicated in Supplementary

Table I. For all data sets, no differences were observed between sexes; therefore, males and females were combined. We determined significance at the threshold of at least 80% power and a *p*-value = 0.05 or less. Data are reported as the mean ± SEM (parametric) or median and range (non-parametric) with individual animals as points within the bar graph. Detailed descriptive statistics and comparisons for every figure are reported in SupplementaryTable I.

3. Results

3.1. Infarct characterization and BBB disruption

This is the first study to evaluate functional outcomes in a cerebellar stroke model, therefore our initial goal was to validate that we could achieve cerebellar infarction that was reproducible and showed characteristic signs of histopathological and pathophysiological injury after stroke (Paz et al., 2010). The cellular architecture is highly conserved throughout the cerebellum; therefore, injury progression, glial reactivity and BBB disruption were evaluated using a single SCA coordinate.

Infarcts.—To assess injury progression and size we performed infarct quantification after photo-thrombotic surgery (Fig. 1a and b) with stereology analysis of H&E stained coronal sections at 1 and 7 days after posterior strokes (Fig. 1c). Results demonstrate infarct production with a significantly greater volume size was observed 1 day after stroke compared to sham [sham: 0.01231 ± mm^3 vs. posterior stroke 1 day: 1.377mm^3, $p < 0.0001$] (Fig. 1d). Infarct size was also measured at 7 days after stroke, and remained significantly different from sham [sham: 0.01231 vs. posterior stroke 7 days: 0.6462mm^3, $p < 0.0001$] (Fig. 1d). No significant differences in infarct volume were found between 1- and 7-day time points after stroke [stroke 1 day: 1.377 vs. stroke 7 days: 0.53877, $p = 0.5387$] (Fig. 1d). Our infarct data are consistent with a previous report demonstrating rapid infarct progression in the cerebellum following photo-thrombotic stroke (Gorlamandala et al., 2018). In addition, an estimated volume of healthy tissue, excluding the infarcted area, was also evaluated with a one-way ANOVA. A trending, but not significant difference, was found between healthy tissue from sham and 1-day animals [sham: 16.25 ± 0.5188 mm^3; vs. 1 day: 14.09 ± 0.9927 mm^3, $p = 0.0690$]. No significant differences were found between sham and 7 days [sham: 14.09 ± 0.9927 mm^3 vs. 7 days: 15.03 ± 0.4683 mm^3, $p = 0.188$], or 1 and 7 days [1 day: 14.09 ± 0.9927 mm^3 vs. 7 days: 15.03 ± 0.4683 mm^3, $p = 0.6342$] (Fig. 1e).Total tissue (healthy plus infarcted) was also calculated to show even representative cerebellar tissue volume across groups [sham: 16.25 ± 0.5188 mm^3 vs. stroke 1 day: 16.04 ± 1.116 mm^3, $p = 0.9778$ vs. stroke 7 days: 15.78 ± 0.4464, $p = 0.8879$] and between time points [stroke 1 day: 16.04 ± 1.116 vs. stroke 7 days: 15.78 ± 0.4464 mm^3 $p = 0.9664$] (Fig. 1f). These results provide good evidence of reproducibility in producing cerebellar infarction using photo-thrombosis, allowing us to further evaluate pathophysiological changes in our model.

Blood Brain Barrier (BBB).—Vascular occlusion due to stroke causes damage to local vasculature compromising the integrity of the blood brain barrier (BBB) and allowing for permeation of molecules, such as albumin, that are normally restricted from the parenchyma, (Radu and Chernoff, 2013). To assess if our cerebellar stroke model caused BBB disruption, we used Evans blue, a dye known for binding strongly to albumin (Radu and Chernoff,

2013) and injected our mice intraperitoneally 1 day after posterior stroke or sham surgery. Brains were perfused collected 4 h post-injection and Evans blue extravasation was present in the ipsilateral cerebellar cortex of stroke mice but not in the contralateral hemisphere or in shams (Fig. 2a). Evans blue concentration could not be quantified from cerebellar tissue as the presence of Rose Bengal dye used for inducing the stroke also leaks through BBB and interfered with Evans blue absorbance wavelength in the spectrophotometer. Therefore, for quantitative analysis of BBB disruption, we injected ovalbumin-Alexa647, also at 1 day after posterior stroke or posterior sham surgery, and collected brains 4 h post-injection. Sections were co-stained with endothelial cell marker, Glut-1 to visualize cerebral vasculature (Fig. 2b). Peri-vascular ovalbumin, was visible in ipsilateral cerebellar sections of stroke animals compared to sham. Our analysis also showed ovalbumin fluorescence (percentage of positive pixels) was >20-fold higher in the ipsilateral cerebellum compared to shams [sham: 0.0624% vs. posterior stroke 1 day (ipsilateral): 1.45%, $p = 0.0112$] (Fig. 2c). Results also show a significant difference between ipsilateral and contralateral hemispheres within the cerebellar stroke group [posterior stroke 1-day (contralateral): 0.0652%, $p = 0.0486$] (Fig. 2c). No significant differences were found between the contralateral hemisphere at 1-day post-stroke and sham ($p > 0.9999$).

Astrogliosis.—We then interrogated whether our cerebellar stroke model showed injury-induced astrogliosis at 1 and 7 days after a posterior stroke. To assess glial reactivity, cerebellar sections from sham and stroke animals were stained for glial fibrillary acidic protein (GFAP) (Fig. 2d). We observed a significant increase in % of positive pixels of GFAP immunoreactivity in the ipsilateral side of animals at 7 days after stroke compared to control [sham: 0.6070% vs. stroke 7 days (ipsilateral): 20.74%, $p = 0.0049$], while no significant differences were found between sham and stroke 7 days (contralateral) [stroke 7 days (contralateral): 1.501%, $p = 0.4947$]. Similarly, no significant differences were found when comparing sham to 1 day stroke (ipsilateral) [stroke 1 day (ipsilateral): 3.460%, $p = 0.4237$] or to 1 day stroke (contralateral) [stroke 1 day (contralateral): 0.2460%, $p > 0.9999$] (Fig. 2e). No differences in BBB or gliosis were observed between posterior and anterior infarcts at any time point (data not shown).

3.2. Infarct comparison between anterior and posterior strokes at 7 days

Strokes to anterior or posterior regions of the cerebellum have been associated with motor and/or cognitive deficits, respectively (Stoodley et al., 2016). We investigated whether our mouse model could also dissociate these deficits based on injury location by restricting illumination to either anterior or posterior lobules of the cerebellar cortex. Laser speckle imaging confirmed a loss of blood flow in the targeted portions of the SCA (Supplementary Figure Ic). To determine the reproducibility of both types of infarcts at 7 days, we first assessed lesion volume via MRI scanning and stereology analysis (Fig. 3). Representative images from anterior and posterior strokes within cerebellar cortex are shown at 7 days. Infarct volumes and water content in the cerebellum of live mice 7 days after either type of stroke were also quantified via MRI diffusion-weighted imaging (Fig. 3b and c). Results show presence of infarction in both groups compared to control [sham: 0 mm3; vs. anterior: 1.070 mm^3, $p = 0.0204$; and vs. posterior: 2.430mm^3, $p = 0.0322$] (Fig. 3b). Water content as a result of edema (Fluri et al., 2015) was significantly greater than shams for both anterior

and posterior infarcts [sham: 0.8240 ± 0.0128 mm^2/s vs. anterior: 1.022 ± 0.06010128 mm^2/s, $p = 0.0238$; and vs. posterior: 1.038 ± 0.081380128 mm^2/s, $p = 0.0369$] (Fig. 3c). Stereological analysis of infarct volume in H&E stained sections was also performed [sham: 0.0123mm^3 vs. posterior stroke 7 days: 0.642mm^3, $p < 0.0001$; and vs. anterior stroke 7 days: 0.2670mm^3, $p = 0.0227$] (as shown in Supplementary Figure Ib). While posterior strokes appeared to produce slightly larger infarct sizes than anterior strokes, these differences were not significant (MRI: $p > 0.9999$, H&E: $p = 0.0889$). H&E stained sections were also used to determine range and extent of damage between the types of infarction. Infarcted tissue was identified and recorded per lobule across animals, anterior (Fig. 3d and f, $n = 8$) and posterior lesions (Fig. 3e and g, $n = 7$) with percentages indicating number of animals per group that show presence of injury. For anterior lesions, although only lobules IV-V were primarily targeted, the damage extended slightly towards a portion of lobule VI due to light dispersion in tissue. For posterior lesions, the damage was confined to portions of the targeted lobules VI-VII and Crus II (cII), extending into lobule VIII. The degree of damage in each lobule (mild, moderate and severe) is described in Supplementary Figure Ia and Supplementary Figs. IIa and IIb.

3.3. Hippocampal plasticity following cerebellar stroke

The cerebellum has direct and indirect reciprocal projections to various areas of the forebrain such as motor, parietal and prefrontal cortices. These anatomical projections from the cerebellum to forebrain are known to decussate contralaterally, including indirect projections to hippocampus, which have just begun to be elucidated (Bohne et al., 2019; Watson et al., 2019). Many higher order memory processes occur within the hippocampus. Given clinical symptoms related to learning and memory dysfunction, we sought to investigate whether cerebellar strokes in mice could impair hippocampal function. Hippocampal plasticity or long-term potentiation (LTP) is a well-known molecular and cellular correlate for learning and memory ex-vivo. Therefore, we evaluated synaptic plasticity in both hippocampi—ipsilateral and contralateral to our unilateral cerebellar stroke (Fig. 4a). Acute hippocampal slices were prepared for field recording experiments from mice subjected to anterior stroke, posterior stroke, or sham surgery. Baseline field excitatory post-synaptic potentials (fEPSPs, normalized to 100%) were recorded from the CA1 region while stimulating CA3 Schaffer collaterals (purple fibers) (Fig. 4b). LTP was evaluated for 60 mins after theta burst stimulation (TBS). The time course of changes in EPSP slopes resulting from TBS are shown for all three groups (anterior, posterior and sham animals) (Fig. 4c and e). Slope values over the last 10 min of every recording were normalized to their own baseline to perform statistical comparisons for ipsilateral, contralateral, and sham hippocampi for anterior (Fig. 4d) and posterior cerebellar strokes (Fig. 4f). Animals with anterior cerebellar strokes exhibited LTP comparable to sham in both hippocampi [sham anterior: 176.7% ± 9.9%; vs. anterior ipsilateral: 194.3% ± 14.7%, $p = 0.7618$; vs. anterior stroke contralateral: 179.0% ± 14.6%, $p = 0.91$] (Fig. 4d). Interestingly, only contralateral hippocampi from mice subjected to posterior cerebellar strokes, show a significant deficit in synaptic potentiation compared to ipsilateral hippocampus and sham [sham posterior: 176.7% ± 9.9% vs. posterior contralateral: 118.5% ± 6.7%, $p = 0.002$; vs. posterior ipsilateral: 155.0% ± 6.3%, $p = 0.05$] (Fig. 4e and f). Linear regression of input/output curves and paired pulse facilitation values show no difference among groups

(Table 1), indicating that intrinsic properties of hippocampal excitatory transmission among groups is undisturbed following either anterior or posterior cerebellar stroke. We used IHC to further investigate if the impairment in synaptic potentiation detected in the CA1 region of the contralateral hippocampus of mice with posterior strokes could be attributed to a reduction in the number of pyramidal neurons or the presence of a microglial or astrocytic inflammatory response 7 days post-stroke. Sections from shams, anterior, and posterior cerebellar groups were processed and stained with NeuN, Iba1, GFAP, respectively. Representative figures of only the contralateral side per group are shown (Fig. 4g). Results showed no differences in % of positive pixels when comparing NeuN staining between sham and posterior stroke [sham contra: 12.94% ± 1.659% vs. posterior contra: 13.89 ± 1.225%, $p > 0.9999$] (Fig. 4h). Similarly, neither Iba1 [sham contra: 0.5334% ± 0.09886% vs. posterior contra: 0.4594% ± 0.0972%, p > 0.9999] (Fig. 4i) nor GFAP [sham contra: 7.736% ± 0.9348% vs. posterior contra: 7.279% ± 0.3125%, p > 0.9999] (Fig. 4j) expression show significant differences from sham. Overall, no significant differences were found across groups, regardless of evaluating contralateral or ipsilateral sides (see Supplementary table I) suggesting a lack of hippocampal pathophysiology.

3.4. Behavioral assessments after cerebellar stroke

We then asked the question if mice with posterior cerebellar lesions that presented impaired LTP in one hippocampus show memory deficits in behavioral studies. To evaluate memory function, mice with sham and cerebellar stroke surgeries were subjected to a contextual fear conditioning task. Freezing behavior is indicative of the animal's capacity to remember and associate the spatial context with the mild foot shock (Fig. 5a). Our analysis showed comparable percentage of freezing behavior between animals with anterior strokes and shams [sham: 65.84% ± 6.734% vs. anterior stroke 7 days: 63.88% ± 4.922%, $p = 0.9644$] (Fig. 5b). Also, there were no significant differences displayed by animals with posterior strokes when compared to sham [sham: 65.84% ± 6.734%; vs. posterior stroke: 66.97% ± 4.297%, $p = 0.9885$]. In addition, no significant differences were found between anterior and posterior group (Fig. 5b).

To corroborate these results, a different cohort of mice with posterior strokes and sham surgeries were subjected to a delayed fear-conditioning assay using an auditory conditioned stimulus (Fig. 5c) which can have a different response to hippocampal perturbations than the non-cued fear conditioning and also allows for evaluation of amygdala-function within the same paradigm. A plotted line graph shows an overview of the results between groups (Fig. 5d). Statistical group comparisons showed no differences in baseline freezing behavior between groups during habituation time in the home cage [sham: 0% vs. posterior: 0%, $p = 0.7093$] (Fig. 5e). Mice were then introduced into context A and similar baseline freezing was observed in this new context [sham: 0% vs. posterior stroke: 0%, $p = 0.8531$] (Fig. 5f). After 2 min in context A, mice received 3 cycles of a conditioned stimulus (CS-auditory cue), paired with an unconditioned stimulus (US-a mild foot shock), triggered at the end of the CS. During this training period, freezing behavior was also evaluated with an unpaired *t*-test and no significant differences were found [sham: 35.65 ± 8.110% vs. posterior: 45.42 ± 4.974%, $p = 0.3247$] (Fig. 5g). The following day mice were introduced back to context A for testing, and no significant differences were found between groups [sham: 64.83 ±

5.162% vs. posterior stroke: 58.94 ± 8.318%, $p = 0.5584$] (Fig. 5h). On the third day mice were introduced to a different environment, context B, where another initial freezing baseline for generalized fear was obtained in this new context. We observed a trending increase in generalized fear in posterior stroke mice [sham: 5.952 ± 1.881 vs. posterior: 12.13 ± 2.774, $p = 0.0901$] (Fig. 5i). Lastly, the same CS delivered in day one was triggered again after 2 mins in context B, and no significant differences were found [sham: 54.64 ± 6.388 vs. 41.82 ± 8.903, $p = 0.2647$] (Fig. 5j). Overall, these data suggest no effect of anterior or posterior stroke on hippocampal- or amygdala- dependent fear memory.

We further evaluated hippocampal function using a recognition memory task, NOR, performed in a 3-chamber apparatus (Fig. 5k,l). Time spent exploring a novel and familiar object was converted into a discrimination index of 0 to 1, to account for any biased preference during the training session. Animals with posterior lesions spent significantly less time exploring the novel object compared to the sham [sham: 0.7865 ± 0.0397 vs. posterior: 0.4118 ± 0.0788, $p = 0.0059$] (Fig. 5m). While there was a trending decrease, no significant differences were found between sham and the anterior stroke group [sham: 0.7865 ± 0.0397 vs. anterior: 0.5408 ± 0.0759, $p = 0.0869$]. No significant differences between and anterior and posterior cerebellar stroke were found [$p = 0.9950$]. These results suggest that a posterior cerebellar stroke impairs recognition memory.

Finally, to address whether anterior or posterior cerebellar stroke affected motor function, mice were subjected to a motor coordination test on a balance beam (Fig. 5n). Interestingly and in contrast with our cognitive evaluation, statistical significance in the number of missteps was found between anterior and posterior cerebellar strokes compared to sham, indicating a lack of coordination and balance [sham: 0 vs. anterior: 6.5, $p < 0.0001$] (Fig. 5o). Significant differences were also found between anterior and posterior stroke groups [anterior: 6.6 vs. posterior: 2, $p = 0.0258$]. In contrast, mice with posterior cerebellar strokes show a similar number of missteps as sham [sham: 0 vs. posterior: 2, $p = 0.1243$] (Fig. 5o). To rule out a lack of mobility of anterior stroke mice that could interfere with motor evaluation, an open field evaluation was done (Fig. 5p) where total distance traveled was evaluated across groups and no differences were found [sham: 46.30 ± 1.482 m vs. anterior: 40.53 ± 4.928 m, $p = 0.4728$; sham: 46.30 ± 1.482 m vs. posterior: 41 ± 3.145 m, $p = 0.5453$; anterior: 40.53 ± 4.928 vs. 41 ± 3.145 m, p = 0.9950] (Fig. 5q). Speed and time spent in inner and outer zones was also evaluated and no significant differences were found (data not shown). These data show that motor coordination and balance can be affected by a unilateral anterior stroke, localized to anterior lobules IV-V and not to posterior lobules VI-VIII.

4. Discussion

Our results demonstrate the ability to induce stroke pathophysiology in targeted cerebellar lobules to evaluate region-specific symptomatology. We observed a dissociation of anterior and posterior functions of the cerebellum that partially mimics the clinical lesion-symptom mapping in cerebellar stroke patients. Hippocampal plasticity impairments were only observed in the posterior cerebellar stroke group and not the anterior. Furthermore, recognition memory was impaired while fear-induced memory was unaffected in posterior

cerebellar mice, suggesting a different sensitivity to the functional changes to the network initiated at the cerebellar level. Similarly, motor deficits were only observed in mice with infarcts in the anterior lobules of the cerebellum. To our knowledge, this is the first report of cerebellar perturbations altering hippocampal plasticity impairments that likely contribute to the observed memory deficit. However, intact function in the ipsilateral hippocampus is likely sufficient to allow for acquisition of fear-induced memory.

4.1. Cerebellar-hippocampal interactions

Our electrophysiological data in posterior cerebellar stroke mice showing a contralateral LTP impairment with no evidence of hippocampal pathophysiology, suggest deficits are likely associated with changes to the cerebellar projections to the forebrain after cerebellar stroke. There is recent evidence of indirect multi-synaptic projections from cerebellum to hippocampus via the ventral thalamus, hypothalamus, medial septum, and raphe nucleus (Bohne et al., 2019; Watson et al., 2019). Retrograde tracing with a rabies virus from injections performed in CA1 of the hippocampus have shown cerebellar labeled cells in posterior lobules VI-VII, indicating anatomical connectivity of these areas with the hippocampus (Bohne et al., 2019; Watson et al., 2019). In our lesion mapping, we found posterior targeting produced mild (damage to granular cell layer) to severe (damage to entire lobule including the molecular layer) damage in lobules VI, VII, VIII of the vermis and lateral lobules Crus I and Crus II (Supplementary Figure IIa and IIb). Functional connectivity of the cerebellum with anterior lobules has also been suggested in optogenetic studies where midline stimulation of lobules IV/V altered cFos expression and calcium events and impaired object location-memory task (Zeidler et al., 2020).The translational significance of cerebellar-hippocampal connectivity has been demonstrated in temporal lobe epilepsy models, where opto-genetic stimulation of Purkinje cells and inhibitory interneurons decreases output of the cerebellar nuclei and reduce seizures in the hippocampus (Krook-Magnuson et al., 2014). While our studies demonstrate a disruption in hippocampal function following posterior cerebellar stroke, further studies are needed to elucidate the mechanism for unilateral LTP impairment found in our study.

We have previously demonstrated bilateral LTP impairments following global or focal forebrain ischemia were associated with impaired fear memory acquisition (Orfila et al., 2019). The unilateral LTP deficits observed in posterior cerebellar stroke mice correlated with an impairment in hippocampal-dependent recognition, but not fear memory. There are examples of unilateral inactivation (Cimadevilla et al., 2005) or lesioning (Li et al., 2012) of the hippocampus resulting in deficits in a Morris Water Maze spatial memory task while others have reported plasticity in one hemisphere is sufficient to support some hippocampal-dependent behaviors but not others. (Wong et al., 1999). It is possible that fear-memory formation may be less sensitive to the unilateral plasticity impairment than the NOR task. It is also possible that differences in fear- and recognition-memory outcomes after posterior cerebellar stroke are not solely dependent on hippocampal function but also on changes in other brain areas that are involved in these tasks. NOR is a non-spatial declarative memory task (Antunes and Biala, 2012; Arias et al., 2015) that has been shown to be sensitive to hippocampal perturbations when administered with an interval of greater than 10 min between training and testing, while shorter intervals are more reflective of perirhinal cortical

function (Cohen and Stackman Jr., 2015). Here, we used an interval of 30 min to evaluate hippocampal-dependent recognition memory, a time period that is more reflective of our ex vivo LTP recordings that evaluate plasticity for up to 1 h after stimulation. Further, the CFC task is also not a purely hippocampal task and also involves other brain regions, including the amygdala. The lack of CFC deficit in our posterior cerebellar stroke model was somewhat surprising, and we therefore validated this result using a cued version of this task, allowing us to evaluate hippocampal- and amygdala-dependent fear memory. Our results suggest that a posterior cerebellar stroke induced alterations to hippocampal LTP, but does not alter fear-memory circuits. Given the unilateral impairment and selective deficits in object recognition, our data suggest that posterior cerebellar stroke causes a mild hippocampal impairment that likely contributes to cognitive disfunction observed in cerebellar stroke patients. Certainly, additional behavioral paradigms will be required in future studies to more broadly assess other cognitive and affective behaviors following cerebellar stroke.

4.2. Motor functions of the cerebellum

Clinical symptomatology related to cerebellar stroke is varied as are the size and locations of infarcts. Lesion-symptom mapping studies confine motor function of the cerebellum to anterior lobules (III-VI) with anterior infarcts causing ataxia and poor fine motor performance. Clinical studies suggest that infarcts localized to lobules VI to X cause minimal to no motor impairments in patients (Schmahmann 2009; Stoodley 2016). Our targeting of cerebellar lobules with photo-thrombosis was able to replicate the dissociation of motor functions to anterior lobules. We did not observe a statistical change in motor function in mice with posterior infarct, however there were mice in the posterior cerebellar stroke group that exhibited more missteps. It is possible that the larger size of our posterior strokes also affected motor regions. Our assessment of motor function was limited to gross locomotion and coordination using the open field and balance beam, respectively. A more thorough behavioral assessment is needed in the future to evaluate other aspects of motor function that may be affected by cerebellar infarct such as skilled reach and motor learning. Nonetheless, we have introduced a novel model for investigating motor deficits after cerebellar stroke that can be used for pre-clinical translational studies.

4.3. Histopathology and pathophysiology of injury

Very few studies have used the photothrombotic approach to generate ischemic infarcts in areas other than sensory-motor cerebral cortex. Our data demonstrate that a cerebellar stroke photothrombotic model is consistent with what has been reported in forebrain stroke, resulting in a similar time course of injury progression and other pathophysiological hallmarks of stroke, including BBB leakage at 24 h (Weber et al., 2020) and astrogliosis (Paz et al., 2010; Fluri et al., 2015). While the photo-thrombotic model of stroke lacks reperfusion typical in rodent transient middle cerebral artery occlusion models, it provides a valuable tool to study long-term functional and network consequences of cerebellar infarction. In fact, the subtle and non-specific nature of cerebellar symptoms (vertigo, dizziness, nausea, headache) often result in delayed diagnosis of cerebellar stroke (Edlow et al., 2008) that would likely exclude them from reperfusion therapies that must be delivered within 4–6 h of stroke onset. Therefore, the permanent occlusion produced in our model

is more likely to resemble the clinical scenario. All surgical parameters were maintained across groups, however, minor differences in infarctions may be attributed to differences in bone thickness–thinner on the posterior side under trapezius muscle-—interfering with light penetration (See Supplementary Figure Ia).

Altogether, our model shows cognitive and motor deficits based on infarct location along with evidence of infarct reproducibility, inflammation in response to injury and blood brain barrier disruption. This mouse model could be a resourceful tool to understand the network alterations that occur after cerebellar stroke and to identify novel mechanisms that can be targeted to improve functional outcomes for patients with this pathology. Future studies will aim to determine how cerebellar stroke alters the cerebello-thalamo-cortical pathways, as well as assessing other motor and cognitive-affective behaviors.

Supplementary Material

Refer to Web version on PubMed Central for supplementary material.

Sources of funding

RO1 NS105905 (NQ); AHA 833684 (MM); RO1 NS105905-S1 (CM); R01 NS046072-S1 (JV); K08 NS086969 (RD); F31 NS120422 (AB). We thank the Colorado Small Animal Imaging Core for providing equipment and scanner time (NCI P30 CA046934 and NIH S10 OD023485, Natalie Serkova, Colorado Animal Imaging Shared Resource). We thank Bryan C. Swanton for his assistance with biostatistics.

Abbrevation:

SCA	Superior Cerebellar Artery
CCAS	Cerebellar Cognitive-Affective Syndrome
RB	Rose Bengal
BBB	Blood-Brain Barrier
MRI	Magnetic Resonance Imaging
BB	Balance Beam
CFC	Contextual Fear Conditioning
DFC	Delay Fear Conditioning
NOR	Novel Object Recognition
fEPSP	*field* Excitatory Post-Synaptic Potential

References

Antunes M, Biala G, 2012. The novel object recognition memory: neurobiology, test procedure, and its modifications. Cogn. Process 13, 93–110. [PubMed: 22160349]

Arias N, Mendez M, Arias JL, 2015. The recognition of a novel-object in a novel context leads to hippocampal and parahippocampal c-Fos involvement. Behav. Brain Res 292, 44–49. [PubMed: 26072392]

Bodranghien F, Bastian A, Casali C, Hallett M, Louis ED, Manto M, Marien P, Nowak DA, Schmahmann JD, Serrao M, Steiner KM, Strupp M, Tilikete C, Timmann D, van Dun K, 2016. Consensus paper: revisiting the symptoms and signs of cerebellar syndrome. Cerebellum 15, 369–391. [PubMed: 26105056]

Bohne P, Schwarz MK, Herlitze S, Mark MD, 2019. A new projection from the deep cerebellar nuclei to the Hippocampus via the ventrolateral and Laterodorsal thalamus in mice. Front. Neural. Circ 13, 51.

Buckner RL, 2013. The cerebellum and cognitive function: 25 years of insight from anatomy and neuroimaging. Neuron 80, 807–815. [PubMed: 24183029]

Carter RJ, Morton J, Dunnett SB, 2001. Motor coordination and balance in rodents. Curr. Protoc. Neurosci 15 (1), 8.12.11–18.12.14.

Choe KY, Sanchez CF, Harris NG, Otis TS, Mathews PJ, 2018. Optogenetic fMRI and electrophysiological identification of region-specific connectivity between the cerebellar cortex and forebrain. Neuroimage 173, 370–383. [PubMed: 29496611]

Cimadevilla JM, Miranda R, Lopez L, Arias JL, 2005. Partial unilateral inactivation of the dorsal hippocampus impairs spatial memory in the MWM. Brain Res. Cogn. Brain Res 25, 741–746. [PubMed: 16216479]

Cohen SJ, Stackman RW Jr., 2015. Assessing rodent hippocampal involvement in the novel object recognition task. A review. Behav. Brain Res 285, 105–117. [PubMed: 25169255]

Desmond JE, Fiez JA, 1998. Neuroimaging studies of the cerebellum: language, learning and memory. Trends Cogn. Sci 2, 355–362. [PubMed: 21227232]

Dietz RM, Orfila JE, Rodgers KM, Patsos OP, Deng G, Chalmers N, Quillinan N, Traystman RJ, Herson PS, 2018. Juvenile cerebral ischemia reveals age-dependent BDNF-TrkB signaling changes: novel mechanism of recovery and therapeutic intervention. J. Cereb. Blood Flow Metab 38, 2223–2235. [PubMed: 29611441]

Dingman AL, Rodgers KM, Dietz RM, Hickey SP, Frazier AP, Clevenger AC, Yonchek JC, Traystman RJ, Macklin WB, Herson PS, 2019. Oligodendrocyte progenitor cell proliferation and fate after white matter stroke in juvenile and adult mice. Dev. Neurosci 1–16.

Edlow JA, Newman-Toker DE, Savitz SI, 2008. Diagnosis and initial management of cerebellar infarction. Lancet Neurol. 7, 951–964. [PubMed: 18848314]

Fluri F, Schuhmann MK, Kleinschnitz C, 2015. Animal models of ischemic stroke and their application in clinical research. Drug Des. Dev. Ther 9, 3445–3454.

Gorlamandala N, Parmar J, Craig AJ, Power JM, Moorhouse AJ, Krishnan AV, Housley GD, 2018. Focal Ischaemic infarcts expand faster in cerebellar cortex than cerebral cortex in a mouse Photothrombotic stroke model. Transl. Stroke Res 9, 643–653. [PubMed: 29455391]

Guzik A, Bushnell C, 2017. Stroke epidemiology and risk factor management. Continuum (Minneap. Minn.) 23, 15–39. [PubMed: 28157742]

Hankey GJ, 2017. Stroke. Lancet 389, 641–654. [PubMed: 27637676]

Igloi K, Doeller CF, Paradis AL, Benchenane K, Berthoz A, Burgess N, Rondi-Reig L, 2015. Interaction between Hippocampus and cerebellum crus I in sequence-based but not place-based navigation. Cereb. Cortex 25, 4146–4154. [PubMed: 24947462]

Kilkenny C, Browne W, Cuthill IC, Emerson M, Altman DG, Group NCRRGW, 2010. Animal research: reporting in vivo experiments: the ARRIVE guidelines. J. Gene Med 12, 561–563. [PubMed: 20607692]

Kim HA, Yi HA, Lee H, 2016. Recent advances in cerebellar ischemic stroke syndromes causing Vertigo and hearing loss. Cerebellum 15, 781–788. [PubMed: 26573627]

Koziol LF, Budding D, Andreasen N, D'Arrigo S, Bulgheroni S, Imamizu H, Ito M, Manto M, Marvel C, Parker K, Pezzulo G, Ramnani N, Riva D, Schmahmann J, Vandervert L, Yamazaki T, 2014. Consensus paper: the cerebellum's role in movement and cognition. Cerebellum 13, 151–177. [PubMed: 23996631]

Krook-Magnuson E, Szabo GG, Armstrong C, Oijala M, Soltesz I, 2014. Cerebellar directed optogenetic intervention inhibits spontaneous hippocampal seizures in a mouse model of temporal lobe epilepsy, eNeuro, 1.

Li H, Wu X, Bai Y, Huang Y, He W, Dong Z, 2012. Unilateral lesion of dorsal hippocampus in adult rats impairs contralateral long-term potentiation in vivo and spatial memory in the early postoperative phase. Behav. Brain Res 230, 428–432. [PubMed: 22409972]

Macdonell RA, Kalnins RM, Donnan GA, 1987. Cerebellar infarction: natural history, prognosis, and pathology. Stroke 18, 849–855. [PubMed: 3629642]

McAfee SS, Liu Y, Sillitoe RV, Heck DH, 2019. Cerebellar Lobulus simplex and crus I differentially represent phase and phase difference of prefrontal cortical and hippocampal oscillations. Cell Rep. 27 (2328–2334), e2323.

Orfila JE, Dietz RM, Rodgers KM, Dingman A, Patsos OP, Cruz-Torres I, Grewal H, Strnad F, Schroeder C, Herson PS, 2019. Experimental pediatric stroke shows age-specific recovery of cognition and role of hippocampal Nogo-a receptor signaling. J. Cereb. Blood Flow Metab 271678X19828581.

Paz JT, Christian CA, Parada I, Prince DA, Huguenard JR, 2010. Focal cortical infarcts alter intrinsic excitability and synaptic excitation in the reticular thalamic nucleus. J. Neurosci 30, 5465–5479. [PubMed: 20392967]

Percie du Sert N, Hurst V, Ahluwalia A, Alam S, Avey MT, Baker M, Browne WJ, Clark A, Cuthill IC, Dirnagl U, Emerson M, Garner P, Holgate ST, Howells DW, Karp NA, Lazic SE, Lidster K, MacCallum CJ, Macleod M, Pearl EJ, Petersen OH, Rawle F, Reynolds P, Rooney K, Sena ES, Silberberg SD, Steckler T, Wurbel H, 2020. The ARRIVE guidelines 2.0: updated guidelines for reporting animal research. PLoS Biol. 18, e3000410. [PubMed: 32663219]

Radu M, Chernoff J, 2013. An in vivo assay to test blood vessel permeability. J. Vis. Exp e50062. [PubMed: 23524912]

Rochefort C, Lefort JM, Rondi-Reig L, 2013. The cerebellum: a new key structure in the navigation system. Front. Neural. Circ 7, 35.

Schaar KL, Brenneman MM, Savitz SI, 2010. Functional assessments in the rodent stroke model. Exp. Transl. Stroke Med 2, 13. [PubMed: 20642841]

Schmahmann JD, 1996. From movement to thought: anatomic substrates of the cerebellar contribution to cognitive processing. Hum. Brain Mapp 4, 174–198. [PubMed: 20408197]

Schmahmann JD, Macmore J, Vangel M, 2009. Cerebellar stroke without motor deficit: clinical evidence for motor and non-motor domains within the human cerebellum. Neuroscience 162, 852–861. [PubMed: 19531371]

Stoodley CJ, Schmahmann JD, 2018. Functional topography of the human cerebellum. Handb. Clin. Neurol 154, 59–70. [PubMed: 29903452]

Stoodley CJ, Valera EM, Schmahmann JD, 2012. Functional topography of the cerebellum for motor and cognitive tasks: an fMRI study. Neuroimage 59, 1560–1570. [PubMed: 21907811]

Stoodley CJ, MacMore JP, Makris N, Sherman JC, Schmahmann JD, 2016. Location of lesion determines motor vs. cognitive consequences in patients with cerebellar stroke. NeuroImage Clin. 12, 765–775. [PubMed: 27812503]

Strick PL, Dum RP, Fiez JA, 2009. Cerebellum and nonmotor function. Annu. Rev. Neurosci 32, 413–434. [PubMed: 19555291]

Watson TC, Obiang P, Torres-Herraez A, Watilliaux A, Coulon P, Rochefort C, Rondi-Reig L, 2019. Anatomical and physiological foundations of cerebellohippocampal interaction. Elife 8.

Weber RZ, Gronnert L, Mulders G, Maurer MA, Tackenberg C, Schwab ME, Rust R, 2020. Characterization of the blood brain barrier disruption in the Photothrombotic stroke model. Front. Physiol 11, 586226. [PubMed: 33262704]

Wong ST, Athos J, Figueroa XA, Pineda VV, Schaefer ML, Chavkin CC, Muglia LJ, Storm DR, 1999. Calcium-stimulated adenylyl cyclase activity is critical for hippocampus-dependent long-term memory and late phase LTP. Neuron 23, 787–798. [PubMed: 10482244]

Zeidler Z, Hoffmann K, Krook-Magnuson E, 2020. HippoBellum: acute cerebellar modulation alters hippocampal dynamics and function. J. Neurosci 40, 6910–6926. [PubMed: 32769107]

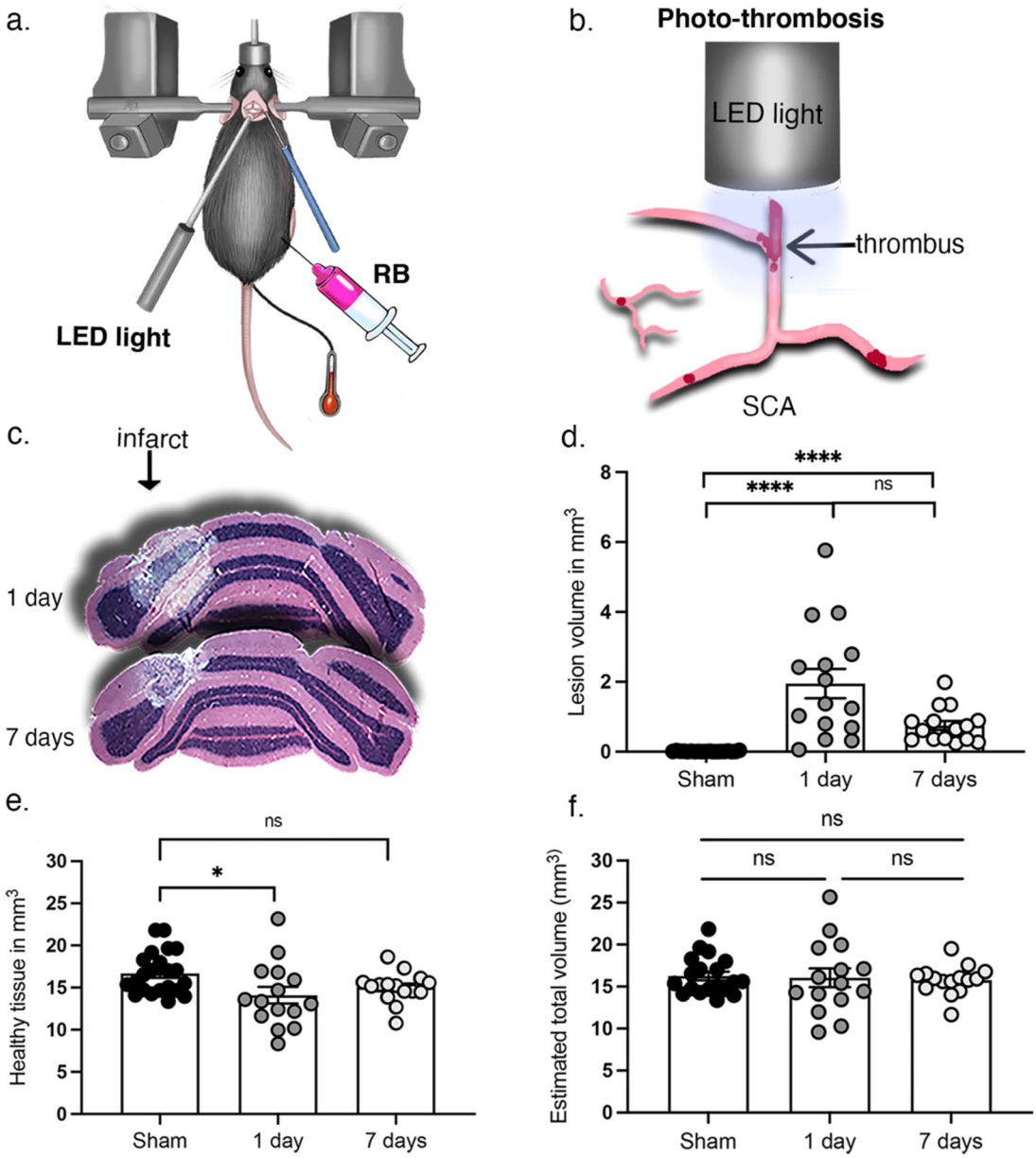

Fig. 1.

Photo-thrombotic stroke of the superior cerebellar artery (SCA) in mice results in infarction to cerebellar cortex. a) Cartoon showing surgery on stereotax and b) LED light inducing the formation of a thrombus in SCA. c) Representative coronal sections from 1 day and 7-days post-cerebellar stroke (posterior type of lesion-infarct pointed with black arrow) after hematoxylin and eosin (H&E) staining. d) Infarct quantification in mm^3 for animals 1 and 7 days after a posterior stroke. e) Healthy cerebellar tissue was measured across groups. f) Total cerebellar volume analyzed for this assay.

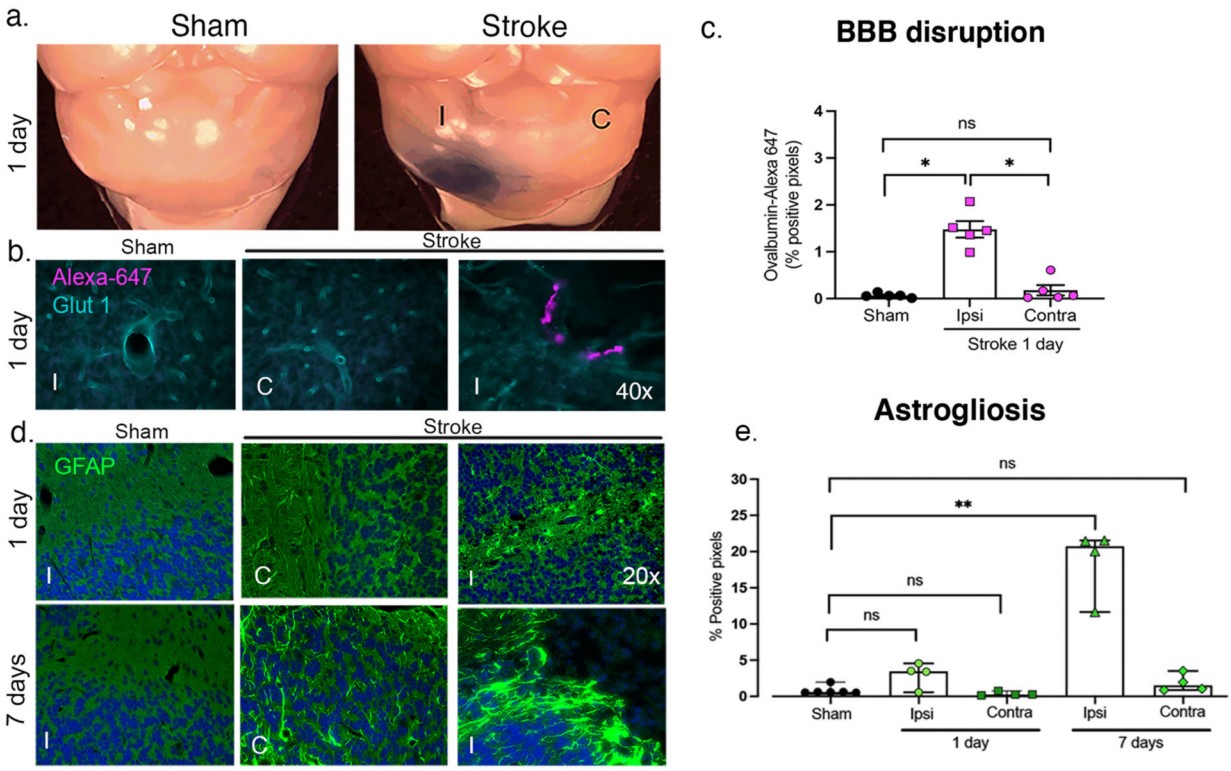

Fig. 2.

Blood brain barrier disruption and astrogliosis at 1 and 7 days after stroke. a) Evans blue extravasation after photo-thrombosis observed in ipsilateral (I) and not contralateral (C) side to injury in a posterior stroke animal and not in sham, 1 day after stroke and 4 h post-injection of Evans blue. b) Representative images from immunohistochemistry assay showing expression of Glut1 co-localization with ovalbumin conjugated with Alexa Fluor-647. c) Relative quantification of ovalbumin volume extravasation through BBB, dots represent averages of multiple images per stroke or sham animals d) Representative images of GFAP in sham ipsilateral side at 1 day and 7 days after surgery and ipsilateral and contralateral sides of stroke after 1 and 7 days. e) Quantification of positive pixels shows significant difference of GFAP expression between stroke ipsilateral, contralateral and sham animals. (For interpretation of the references to colour in this figure legend, the reader is referred to the web version of this article.)

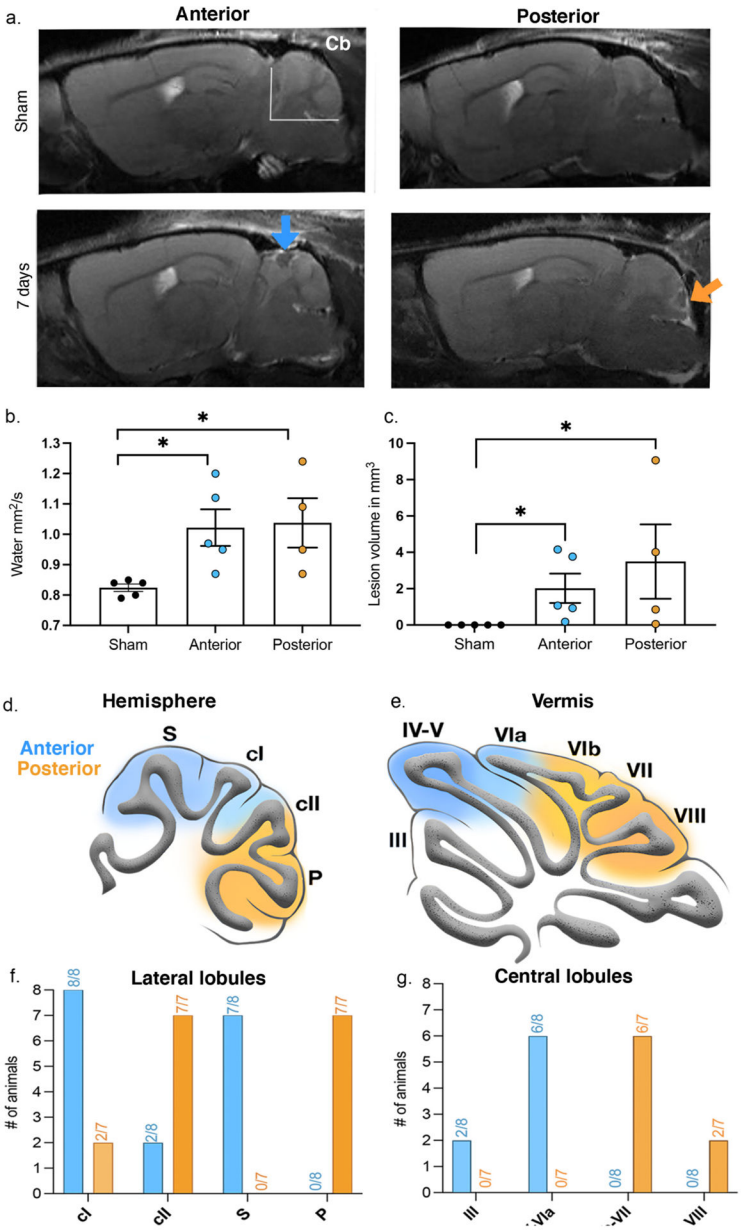

Fig. 3.

MRI analysis and identified damaged lobules per infarct type. a) Representative images of mice after sham, anterior, and posterior stroke surgeries visualized at 7 days. b) Lesion volume (mm^3) and c) water content (mm^2/s) quantification. d and e) Recurrent vermal and lateral lobules damaged after anterior (blue) and posterior (orange) stroke surgeries. f and g) Qualitative analysis of lateral and central lobules predominantly damaged in a cohort of mice with anterior (n = 8) and posterior (n = 7) strokes. (For interpretation of the references to colour in this figure legend, the reader is referred to the web version of this article.)

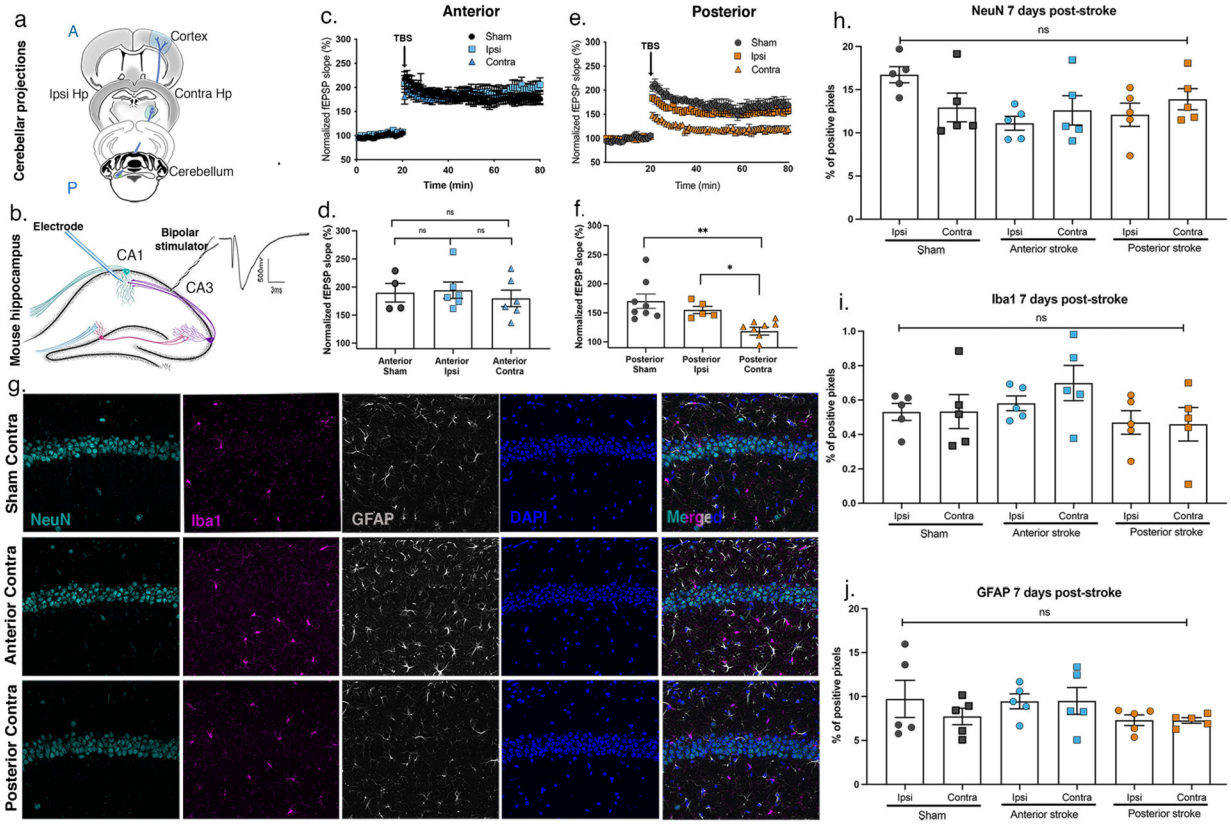

Fig. 4.

Plasticity impairments in contralateral hippocampus 1 week after posterior cerebellar stroke. Recordings were made in acute hippocampal slices from mice after sham, anterior and posterior cerebellar stroke surgeries in a) ipsilateral and contralateral Hp. b) Coronal hippocampal cartoon indicating stimulator in CA3 and recording electrode in CA1, fEPSP on the left. c and e) TBS was delivered to induce LTP (black arrow) (left) for animals with anterior and posterior cerebellar strokes. d and f) Mean normalized fEPSP slope during the last 10 min of recording for each group (* indicates $p < 0.05$). g) Representative images of CA1 layer stained with NeuN, Iba1, GFAP and DAPI. h) Quantified percentage of positive pixels for NeuN, i) Iba1, and j) GFAP and compared among sham, anterior, and posterior groups.

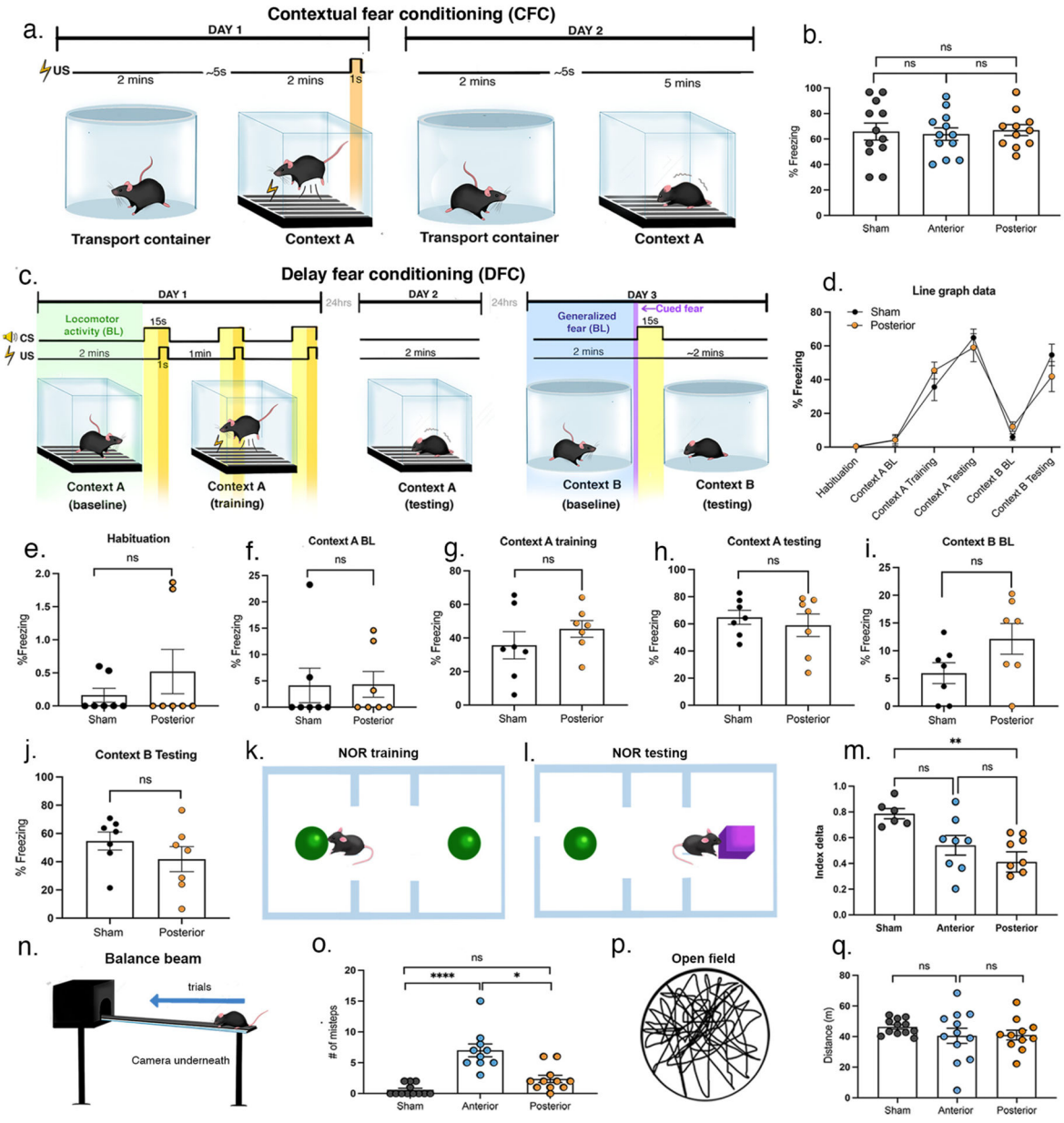

Fig. 5.

Behavioral assessment of cognitive and motor performance 7 days after anterior and posterior cerebellar strokes. a.) Cartoon showing CFC setup for assay over 2 days. b.) Line graph showing results comparing sham, anterior and posterior strokes % time spent freezing. c.) Cartoon showing DFC setup for assay over 3 days. d.) Line graph showing results comparing sham and posterior strokes at each step of the task. e-j.) Freezing percentage quantification for each task. k, l.) Behavioral setup for NOR training and testing. m.) Quantified index delta for novel object preference for each group n.) Balance beam setup for motor performance assay. o.) Quantified number of missteps compared between mice

with sham, anterior, and posterior strokes. p) Representation of an open field trajectory for a single mouse. q.) Total distance traveled per animal per group.

Table 1

PPR and I/O results from LTP data.

Parameter	Sham	Anterior stroke (Ipsi)	Anterior stroke (Contra)	Posterior stroke (Ipsi)	Posterior stroke (Contra)	P value
PPR (pulse2/pulse1)	1.392 ± 0.0779	1.414 ± 0.0665	1.345 ± 0.6118	1.432 ± 0.03601	1.429 ± 0.0496	0.8722
I/O (slope)	2.322 ± 0.1578	2.002 ± 0.1215	2.081 ± 0.1825	2.065 ± 0.1056	1.753 ± 0.1801	0.9952